

Tropical analysis uncertainties and Kelvin waves: what can be learnt from the Aeolus wind profiles?

Nedjeljka Žagar¹, Michael Rennie², and Lars Isaksen²

¹Universität Hamburg, Meteorological Institute

²ECMWF

November 21, 2022

Abstract

The European Space Agency Earth Explorer mission Aeolus with the first spaceborne Doppler Wind Lidar onboard provides the global coverage of wind profiles twice per day. This paper discusses the impact of Aeolus winds on the quality of tropical analyses using the observing system experiments of the European Centre for Medium Range Weather Forecasts. Focusing on a period in May 2020, it is shown that Aeolus winds improve the fit of short-term forecasts to observations for other observations types, in spite of their random errors significantly greater than error estimates for short-term tropical forecasts. It is argued that Aeolus winds lead to more accurate representation of the vertically-propagating equatorial waves in the tropical upper troposphere. Examples of Kelvin waves suggest that analysis increments occur in the layers with a significant vertical shear during the easterly phase of the quasi-biennial oscillation in May 2020.

Tropical analysis uncertainties and Kelvin waves: what can be learnt from the Aeolus wind profiles?

N. Žagar¹, M. Rennie² and L. Isaksen²

¹Meteorologisches Institut, Universität Hamburg, Germany

²European Centre for Medium Range Weather Forecasts, Reading, UK

Key Points:

- Aeolus wind profiles improve tropical analyses in regions of a strong zonal wind shear in the tropical upper troposphere and lower stratosphere (UTLS).
- Aeolus winds are shown to modify the vertically-propagating Kelvin waves in UTLS.
- Impact of Aeolus winds in the ECMWF system in May 2020 is coupled to the easterly phase of the quasi-biennial oscillation.

Corresponding author: Nedjeljka Žagar, Meteorologisches Institut, Universität Hamburg, Germany,, nedjeljka.zagar@uni-hamburg.de

Abstract

The European Space Agency Earth Explorer mission Aeolus with the first spaceborne Doppler Wind Lidar onboard provides the global coverage of wind profiles twice per day. This paper discusses the impact of Aeolus winds on the quality of tropical analyses using the observing system experiments of the European Centre for Medium Range Weather Forecasts. Focusing on a period in May 2020, it is shown that Aeolus winds improve the fit of short-term forecasts to observations for other observations types, in spite of their random errors significantly greater than error estimates for short-term tropical forecasts. It is argued that Aeolus winds lead to more accurate representation of the vertically-propagating equatorial waves in the tropical upper troposphere. Examples of Kelvin waves suggest that analysis increments occur in the layers with a significant vertical shear during the easterly phase of the quasi-biennial oscillation in May 2020.

Plain Language Summary

Tropics are the region with the largest uncertainties in the initial state for numerical weather prediction - analyses. Analysis uncertainties are largest in the upper tropical troposphere and the lower stratosphere (UTLS). One of the reasons is a lack of wind profiles which are more useful than temperature profiles in the tropics. This classical effect was described by Smagorinsky as "Not all data are equal in their information-yielding capacity. Some are more equal than others". In this paper we show the impact of the first global wind profile observations by the ESA's mission Aeolus on the vertically-propagating Kelvin waves. Aeolus winds improve the structure of vertically-propagating waves in the UTLS in regions with the strongest wind shear. This effect is demonstrated on the Kelvin waves in May 2020 during the easterly phase of the quasi-biennial oscillation when shear lines in the tropical tropopause layer were particularly strong. In light of the previous work on the role of Kelvin waves in the tropical atmosphere and their treatment, or a lack of it, in tropical data assimilation modeling, lessons learnt from Aeolus winds can lead to improved assimilation procedures and a reduction of tropical analysis uncertainties.

1 Introduction

Even though progress in numerical weather prediction (NWP) in the past two decades has been tremendous (Bauer et al., 2015) including progress in the simulation of tropical variability (Vitart et al., 2014), the tropics remain a region with the largest analysis uncertainties, especially in the upper troposphere and lower stratosphere (UTLS); here, tropical analysis and short-range forecast uncertainties far exceed uncertainties in the upper-troposphere in mid-latitudes (Park et al., 2004; Žagar, 2017). For example, an inter-comparison of the six state-of-the-art NWP systems by Park et al. (2004) showed that the root-mean-square differences between the analyses over the tropics exceed the climatological standard deviation of the tropical circulation. In contrast, the differences among the same analyses over the extra-tropics make around 10% of the corresponding climatological variability. It is therefore not surprising that the description of synoptic variability in the tropical tropopause layer (TTL) is not reliable. Since variability of the tropical lower stratosphere is largely maintained by vertically propagating equatorial waves, their accurate representation in analyses is vital also for climate model validation (Fujiwara et al., 2012).

Analysis uncertainties in the tropics are associated with model errors, with shortcomings in data assimilation modelling and with a lack of observations, especially observations of wind profiles. In this paper we discuss a positive impact of the first spaceborne measurements of the global wind profiles by Doppler Wind Lidar ALADIN (ESA,

1999, 2008; Reitebuch, 2012), onboard the ESA Earth Explorer mission Aeolus¹, on the quality of tropical analyses. We show that Aeolus wind profiles improve the fit of short-term forecasts to observations for other observations types, in spite of their random errors on average being significantly greater than error estimates for short-term tropical forecasts using the ensembles. We focus on analysis improvements in vertically-propagating equatorial waves in the UTLS region and specifically on the Kelvin wave. By filtering the Kelvin waves from the ECMWF analyses with and without Aeolus winds we demonstrate that Aeolus brings changes to the vertical wave structure in the layers with the strongest wind shear that is observed by Aeolus.

The Aeolus mission (Stoffelen et al., 2005) was under development since late 1990s leading to the successful launch of the Aeolus satellite in August 2018. At ECMWF, Aeolus observations have been used in operations since 9 January 2020. Prior to its operational use, a major effort was invested to validate the new measurements and to understand the origin of biases (Rennie & Isaksen, 2020, 2021). After the bias removal, the random error of Aeolus observations in clear air is still typically about twice that of radiosondes or aircraft wind measurements, because the effective Aeolus laser signal was a factor 2-3 lower than expected pre-launch. Nevertheless, evaluation of Aeolus forecast impact in the ECMWF operational system and observing system experiments show that Aeolus' impact on short-range forecasts has a similar magnitude to that of other satellite observations (Rennie & Isaksen, 2021), this in spite of Aeolus accounting for less than 1% of the assimilated observations. Forecast scores suggest that the largest positive impact of Aeolus winds is in the tropical UTLS region, with improvements in lower-stratosphere temperature forecasts extending to the medium range. Here we present the first evidence that reported improvements in the simulations of tropical circulation are associated with an improved representation of the large-scale equatorial waves in UTLS, in particular the Kelvin wave.

The Kelvin wave (KW) is one of the most studied features of the tropical atmosphere. The KW is the slowest eastward-propagating wave solutions of the linearized primitive equations and therefore the first-order ingredient of the circulation response to tropospheric heating perturbations (Salby & Garcia, 1987), easily detectable in different types of observations (Wheeler & Kiladis, 1999; Alexander & Ortland, 2010; Matthews & Madden, 2000; J. E. Kim & Alexander, 2013). In the stratosphere, where the KW was first discovered as a 15-day wave (Wallace & Kousky, 1968), it effects zonal mean quasi-periodic flows such as the quasi-biennial oscillation (QBO) (Baldwin & Coauthors, 2001), and it is widely considered to play a role in dynamics of the Madden-Julian Oscillation (MJO) (Zhang, 2005). Although the KW is predominantly a planetary-scale wave (zonal wavenumber 1), its analyses can still get occasionally poor even in the stratosphere (Podglajen et al., 2014).

In spite of its approximately non-dispersive nature and geostrophic coupling between the zonal wind the meridional pressure gradient, KW is a significant contributor to tropical analyses uncertainties and forecast errors, and its role in predictability has been addressed by several studies in the past (Žagar et al., 2007, 2013; Žagar, Buizza, & Tribbia, 2015). For example, Žagar et al. (2007) found that the ECMWF forecast errors within 20° N–20° S belt project on KWs significantly more in the easterly QBO phase than in the westerly phase. Žagar et al. (2016) showed that although the upper-troposphere tropical forecast errors grow more rapidly in the balanced modes, the analysis increments at the same levels are larger in unbalanced modes, including the KWs, than in balanced modes, suggesting shortcomings in the analysis of unbalanced tropical circulation. Furthermore, Žagar, Buizza, and Tribbia (2015) showed that missing variance in KWs explains a large part of underdispersiveness of the ECMWF ensemble prediction system in medium range in the tropics. It is unclear how well KW dynamics is

¹ https://www.esa.int/Applications/Observing_the_Earth/Aeolus

111 represented in global climate models, as they still poorly simulate the QBO and MJO,
112 and their connections (H. Kim et al., 2020).

113 In a relatively short time since its launch, and in spite of larger systematic and ran-
114 dom errors than expected pre-launch, Aeolus winds have justified and even exceeded ex-
115 pectations of atmospheric science community. This was only the case after the discov-
116 ery of a strong link between onboard telescope temperatures and systematic wind speed
117 errors (Rennie & Isaksen, 2020, 2021). Aeolus not only led to forecast improvements at
118 several global NWP centres, but was also shown capable of observing gravity waves (Banyard
119 et al., 2021) and providing useful aerosol observations (Baars et al., 2021).

120 Here we use a subset of the results from the ECMWF observing system experiments
121 (OSEs) to investigate the tropical impact of Aeolus winds on process level. We suggest
122 that Aeolus observations improve large-scale, vertically-propagating KWs by adding wind
123 information in the layers of significant vertical shear of the horizontal winds in the trop-
124 ical UTLS layer. In Section 2, we present the method including the evidence of a posi-
125 tive impact of Aeolus winds on the forecast fit to other observations types. Section 3
126 focuses on KW analyses, while Section 4 contains the discussion and outlook.

127 2 Method and Data

128 2.1 Observing System Experiment with Aeolus winds

129 ALADIN instrument onboard Aeolus measures four types of the profiles of the hor-
130 izontal line of sight (HLOS) winds depending on the classification of atmosphere into clear
131 air (Rayleigh winds) or cloudy (Mie winds) (D. Tan et al., 2008). Individual measure-
132 ments with the scale of about 3 km are accumulated to produce profiles representative
133 for up to 86 km scale for Rayleigh-clear, and about 12 km for Mie-cloudy scenarios. In
134 the vertical direction, the atmosphere is divided into 24 layers, so-called range-bins, that
135 have thickness 250-2000 m, and the HLOS wind is assigned to the center of the bin. Val-
136 ues of the Rayleigh-wind with large estimated observation error are rejected based on
137 criteria 12 m/s (8.5 m/s) above (below) 200 hPa. After the bias removal, the random
138 error of Aeolus observations in clear air is found to vary between 4 and 7 m/s for Rayleigh-
139 clear winds and 2.8 to 3.6 m/s for Mie-cloudy winds (Rennie & Isaksen, 2021). The Rayleigh-
140 clear winds below 850 hPa were discarded in these observing impact studies.

141 The OSE was performed for the Aeolus period May to September 2020 using the
142 operational ECMWF system with 137 level up to 1 Pa. The model version was CY47R1.1
143 with the 4D-Var outer loop at resolution TcO399 which corresponds to about 30-km grid
144 distance. The operational system applies the 12-hour continuous 4D-Var (Lean et al.,
145 2021). The experiment which included Aeolus winds on top of all other observations is
146 denoted "Aeolus". The reference experiment with all observations except Aeolus will be
147 referred to as "NoAeolus". Rennie and Isaksen (2021) present the NWP impact assess-
148 ment for the whole OSE period. Here we look at 12 UTC analyses during May.

149 An evidence of the impact of Aeolus winds is presented in Fig. 1 for a 10-day pe-
150 riod, 20-30 May 2020, for the tropical belt 20°S-20°N. A relative improvement in the Ae-
151 olus experiment compared to NoAeolus is shown by the normalised root-mean-square-
152 errors of the short-range forecasts compared to different observation types. This kind
153 of assessment of forecast impact is more suitable than a comparison of forecast with anal-
154 yses for a short period like here. We present the relative fit to zonal wind measurements
155 from radiosondes, AMSU-A microwave radiances, and radio occultation (GPSRO) data,
156 but we also computed (not shown) the fits for the aircraft, Atmospheric Motion Vectors
157 (AMVs), and Japanese wind profilers. For all these observing systems there is a relatively
158 large improvement in these independent observations, shown by values less than 100%
159 in the error curves. The improved fit for the 20-30 May period is larger than seen from
160 the same evaluation in the tropics over an extended period from April to September 2020

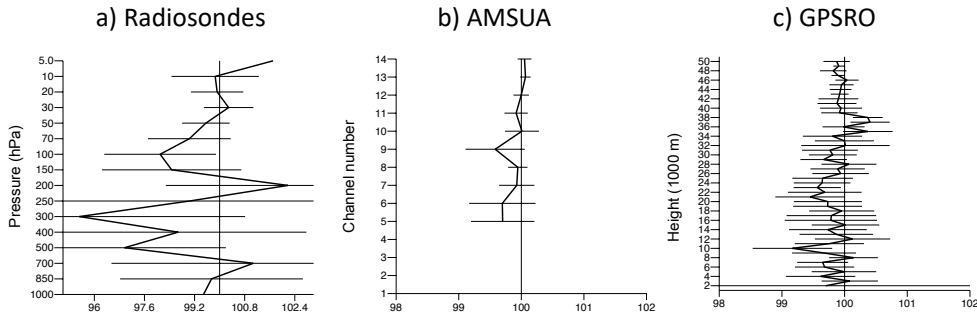


Figure 1. Root mean square errors for zonal winds in the tropics in period 20-30 May, normalised differences between the Aeolus and NoAeolus experiments. Evaluation is for background - observation for a) tropical radiosonde zonal winds, b) different AMSU radiance channels and c) GPSRO bending angle data. Values lower than 100% mean an improvement due to Aeolus winds. The error bars for 95% confidence intervals are included.

161 (not shown). Thus, Fig. 1 shows that using Aeolus winds generally improve forecasts
 162 and analyses.

163 2.2 Kelvin wave filtering

164 The KW is filtered from Aeolus and NoAeolus analyses using MODES (Žagar, Kasa-
 165 hara, et al., 2015) which implements classical linear wave theory in the terrain-following
 166 coordinate system following Kasahara and Puri (1981). MODES simultaneously projects
 167 winds and pseudo-geopotential field defined by temperature and surface pressure on bal-
 168 anced (Rossby) and unbalanced (inertia-gravity) eigensolutions of the linearized prim-
 169 itive equations. The framework is well suited for the KW which is the normal mode of
 170 the global atmosphere. For details of the linear wave filtering, the reader is referred to
 171 Kasahara (2020) and references therein. Filtering of operational ECMWF forecasts² re-
 172 veals the KW signals regularly propagating eastward and upward to the stratosphere with
 173 the strongest tropospheric signal over the Indian ocean and western Pacific as illustrated
 174 in Supplement.

175 3 Aeolus winds and equatorial Kelvin wave

176 3.1 Kelvin wave winds versus balanced winds near the equator

177 KW zonal winds superposed on tropical balanced zonal winds in the NoAeolus and
 178 Aeolus experiments in mid-May 2020 are displayed in Fig. 2. The figure shows westerly
 179 winds in the upper tropical troposphere and within the TTL, except between 60°E and
 180 100°E. In this region, KW winds are about equal or stronger than the balanced wind,
 181 which are also easterlies. The peak altitude of KW over the Indian ocean and in the vicin-
 182 ity of the strongest balanced easterlies are in agreement with the climatological KW struc-
 183 ture in observations and in earlier ECMWF analyses (Suzuki & Shiotani, 2008; Alexan-
 184 der & Ortland, 2010; Flannaghan & Fueglistaler, 2013; Blaauw & Žagar, 2018). The as-
 185 sociated KW temperature perturbations in TTL reach about 1.5 K (Blaauw & Žagar,
 186 2018).

² <https://modes.cen.uni-hamburg.de>

187 An eastward-slanted, vertically propagating KW structure over the Indian ocean
 188 is in a contrast to a weaker KW signal over the western Pacific within a layer of balanced
 189 westerly flow below 100 hPa. Figures in Supplement show that KWs represent the most
 190 of the unbalanced (or non-Rossby) signal. The total zonal flow (Figures in Supplement)
 191 appears far less smooth than the balanced winds because small-scale, divergent struc-
 192 tures project on the inertia-gravity modes. The predominant feature of Fig. 2 is a strong
 193 shear of the zonal wind, both vertical and horizontal. The presence of a strong easterly
 194 wind shear layer between 100 hPa and 80 hPa in May 2020 is associated with the east-
 195 erly QBO phase which is known to provide favourable conditions for intense KW dynam-
 196 ics (Suzuki et al., 2010; Flannaghan & Fueglistaler, 2012).

197 Figure 2 also shows that between 13 May and 16 May 2020, balanced easterlies over
 198 the Indian ocean strengthened, along with strengthening westerlies around the dateline.
 199 An even stronger enhancement of both horizontal and vertical shear occurred in the to-
 200 tal wind (Figures in Supplement). Such strong wind shear is typical for mid-latitude fronts
 201 with Aeolus demonstrated capable of improving their mesoscale features (Šavli et al., 2018).
 202 On synoptic scales in mid-latitudes, the thermal wind balance can be applied to derive
 203 the vertical wind shear from the horizontal temperature gradient, with the temperature
 204 field obtained from high-accuracy measurements of radiances. In the tropics, the weak-
 205 temperature gradient theory for the slow, large-scale motions relies on the smallness of
 206 temperature gradient (Sobel et al., 2001), thereby excluding the KW. However, wher-
 207 ever the Kelvin and Rossby waves are present together near the equator, their zonal winds
 208 will sum up (or subtract) whereas their temperature perturbations will subtract (or sum
 209 up), since their mass-wind couplings have opposite signs. Using the horizontal structure
 210 of mass-field observations to derive the Kelvin and Rossby wave signals near the equa-
 211 tor therefore requires quantification of their respective variances. This is a challenging
 212 task for data assimilation, even in the perfect-model 4D-Var (Žagar, 2004). Direct wind
 213 observations, as argued since early days of the Aeolus project, are crucial to improve ac-
 214 curacy of tropical analyses.

215 3.2 Effects of Aeolus winds on Kelvin waves

216 There is little difference between the NoAeolus and Aeolus experiments in Fig. 2.
 217 An eye inspection suggest that differences are up to the level used for contouring, 3 m/s.
 218 This is not a small value for an experiment in which the only difference is the assimi-
 219 lation of Aeolus winds characterised by a significant random error. To understand trop-
 220 ical dynamical processes affected by Aeolus assimilation, we need to look at differences
 221 between analyses or at analysis increments. The latter shows the effect of observations
 222 in a single assimilation cycle whereas the former includes the effect of observations as-
 223 similated earlier in the experiment. The memory of observations in the tropics should
 224 be longer than in the extratropics (Fisher et al., 2005). Observations that affect the trop-
 225 ical mean state can be expected to have a memory of at least 10 days as it was seen for
 226 Aeolus data and AMSU-A radiance data in reanalyses (not shown). With the focus on
 227 Aeolus effects of vertically-propagating waves and their impact on circulation, we present
 228 differences between analyses with and without Aeolus winds.

229 Figure 3 shows that differences between KWs in the two experiments occur mainly
 230 over the Indian ocean at the locations of the vertical wave propagation and significant
 231 shear. For example, the assimilation of Aeolus winds on 13 May enhanced easterlies near
 232 100 hPa over Indian ocean while on 19 May the KW vertical structure was modified over
 233 a deeper layer. Differences in the TTL are several meters per second. The vertical KW
 234 structure at two locations, 66°E and 90°E, and 3 consecutive days is presented in Fig.
 235 4. It shows the downward propagation of the KW phase from the lower stratosphere across
 236 the TTL. The vertical phase speed at 66°E earlier in the period has a greater amplitude
 237 than at 90°E. The most relevant is the modification of the KW shear between 100 hPa
 238 and 50 hPa where the amplitudes and vertical propagation are the largest.

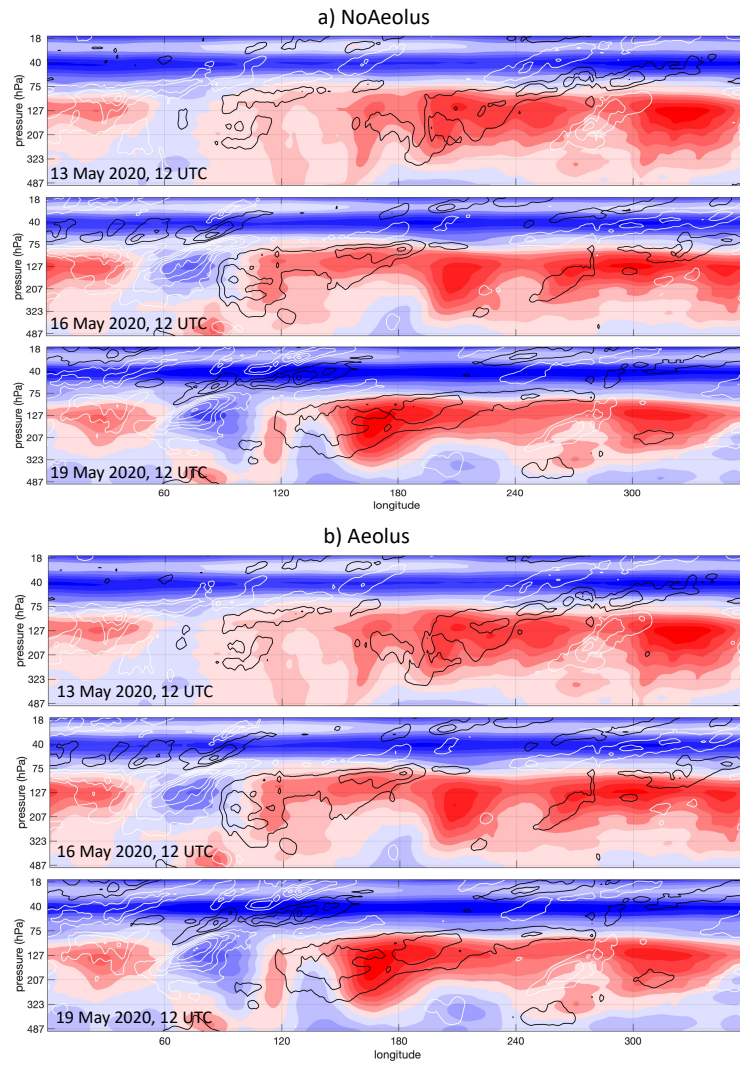


Figure 2. Kelvin wave zonal winds (contours) superposed on the balanced winds (shades) along the equator, averaged over the belt 10°N - 10°S in (a) NoAeolus and (b) Aeolus experiments on 13 May, 16 May and 19 May 2020, 12 UTC. Contouring is every 3 m/s, starting at ± 3 m/s, with black contours for westerly and white contours for easterly Kelvin wave winds. Balanced zonal winds is shaded every 3 m/s, with red shades for westerlies and blue shades for easterlies.

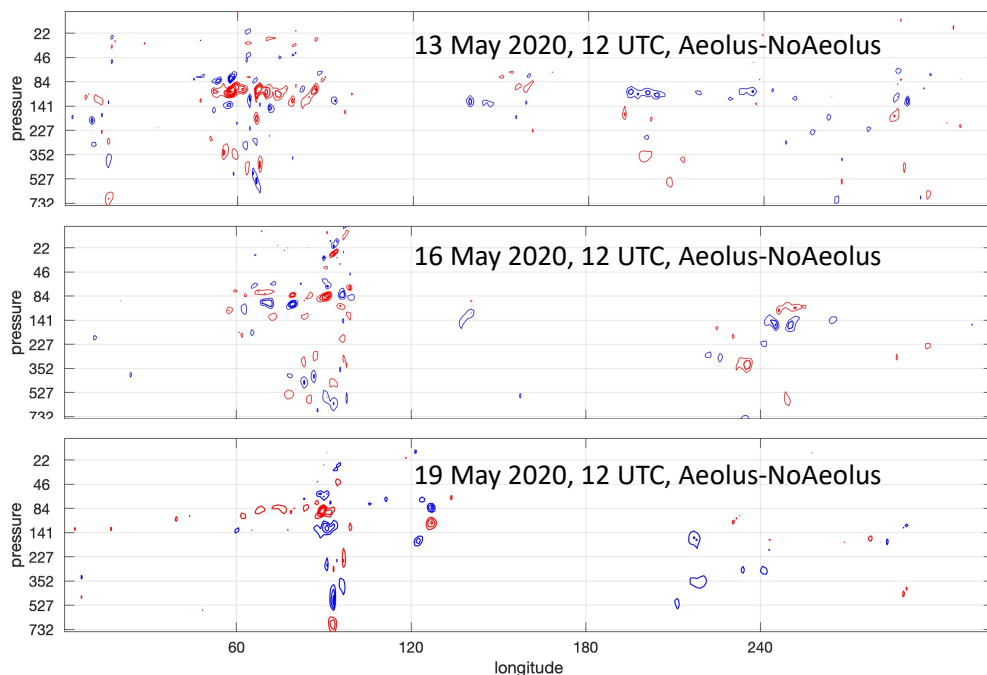


Figure 3. Kelvin wave zonal wind differences along the latitude 0.5°N between the Aeolus and NoAeolus experiments on 13 May, 16 May and 19 May 2020, 12 UTC. Contouring is every 0.5 m/s, starting at ± 1 m/s. Red contours for positive, and blue for negative differences.

239 In contrast to the large portion of the total zonal circulation associated with KWs
 240 (Fig. 2), its analysis increments are relatively small (not shown). This may suggest that
 241 KWs are well represented in forecasts (first-guess fields) in both experiments. However,
 242 evaluation of tropical analysis and forecast uncertainties do not support such an argu-
 243 ment (Podglajen et al., 2014; Žagar, 2017). Total differences partitioned between bal-
 244 anced and unbalanced parts in the NoAeolus and Aeolus analyses show that the two com-
 245 ponents have similar amplitudes in regions and layers of strong shear, where westerlies
 246 shift to easterlies or vice versa. In other regions such as upper troposphere westerlies over
 247 Pacific with a weaker KW signal, differences between Aeolus and NoAeolus are almost
 248 entirely in balanced modes. Details remain for follow-on investigations using the extended
 249 period and sensitivity studies.

250 4 Discussion and Outlook

251 Improvements to the KW analyses due to Aeolus data may not come as a surprise
 252 since Aeolus winds in the tropics are nearly zonal and tropical improvements have been
 253 foreseen (D. G. H. Tan & Andersson, 2004; D. Tan et al., 2007; Žagar, 2004). On the
 254 other hand, during the two decades since the Aeolus project started, NWP experienced
 255 large advancements with improved data assimilation and more observations used, and
 256 the current forecast models routinely run at resolutions around or under 10 km. Yet, prac-
 257 tical predictability in extratropics remains under 10 days (Haiden & Coauthors, 2018),
 258 and tropics-extratropics interactions are argued as one way to improve medium- and extended-
 259 range forecasting (Žagar & Szunyogh, 2020).

260 Our evaluation of the background fit to other observations shows an overall posi-
 261 tive impact of Aeolus winds in the tropics, in spite of large random errors. In fact, the
 262 impact in May was larger than for the whole 6-period experiment April-September (not

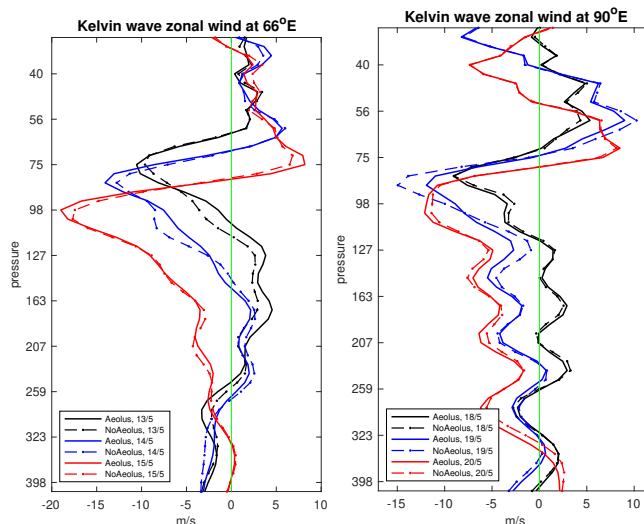


Figure 4. Kelvin wave zonal wind in 12 UTC analyses at three subsequent days in May 2020 in Aeolus (full lines) and NoAeolus (dashed lines) OSEs. The locations are indicated above the panels.

263 shown). A likely reason is the coupling between the forecast errors and the QBO phase
 264 which was stronger in May than in the later part of the OSEs. While the QBO phase
 265 and KWs are not explicitly represented in the background-error term for data assim-
 266 lation in the ECMWF system, the background-error variances are derived using the 4D-
 267 Var ensemble of data assimilation thereby accounting for the flow-dependent amplitudes
 268 of short-range forecast errors in temperature and winds.

269 The impact of Aeolus winds on the KWs is closely coupled to the vertical shear lines
 270 across TTL and regional aspects of tropical circulation. It remains to investigate how
 271 Aeolus winds affect analysis increments in the upper-troposphere and TTL and the dis-
 272 persiveness of the ensemble prediction system. Here presented results suggest that at least
 273 a part of reported forecast improvements in the tropical lower stratosphere (Rennie &
 274 Isaksen, 2021) comes from corrections to the large-scale, vertically-propagating Kelvin
 275 waves in layers with strong wind shear.

276 Acknowledgments

277 We are indebted to the many experts who over years worked on the Aeolus mission un-
 278 til its launch on 22 August 2018, and to many who have been operating the satellite and
 279 contributing to the validation and processing of Aeolus measurements at ESA and within
 280 the DISC team. The source code of the ECMWF IFS model is not available for public
 281 use as it is intellectual property of the ECMWF and its member states. MODES soft-
 282 ware for the linear wave filtering can be requested through [http://modes.cen.uni-hamburg](http://modes.cen.uni-hamburg.de)
 283 [.de](http://modes.cen.uni-hamburg.de). Results of the modal decomposition of ECMWF OSEs discussed in the paper are
 284 available at <https://zenodo.org/record/4942970#.YmkZVi2B0Q8> (doi: 10.5281/zen-
 285 odo.4942970). Archiving the input OSE analyses for the presented period in May 2020
 286 to the same repository is underway.

287 References

288 Alexander, M. J., & Ortland, D. A. (2010). Equatorial waves in High Resolution Dy-
 289 namics Limb Sounder (HIRDLS) data. *J. Geophys. Res.*, *115*, D24111. doi: 10

- 290 .1029/2010JD014782
- 291 Baars, H., Radenz, M., Floutsis, A. A., Engelmann, R., Althausen, D., Heese,
292 B., . . . Wandinger, U. (2021). Californian wildfire smoke over Europe:
293 A first example of the aerosol observing capabilities of Aeolus compared
294 to ground-based lidar. *Geophys. Res. Lett.*, *48*, e2020GL092194. doi:
295 <https://doi.org/10.1029/2020GL092194>
- 296 Baldwin, M. P., & Coauthors. (2001). The quasi-biennial oscillation. *Rev. Geophys.*,
297 *39*, 179-229.
- 298 Banyard, T. P., Wright, C. J., Hindley, N. P., Halloran, G., Krisch, I., Kaifler, B.,
299 & Hoffmann, L. (2021). Atmospheric Gravity Waves in Aeolus Wind Li-
300 dar Observations. *Geophysical Research Letters*, *48*, e2021GL092756. doi:
301 <https://doi.org/10.1029/2021GL092756>
- 302 Bauer, P., Thorpe, A., & Brunet, G. (2015). The quiet revolution of numerical
303 weather prediction. *Nature*, *525*(47), 10.1038/nature14956. doi: [https://doi](https://doi.org/10.1038/nature14956)
304 [.org/10.1038/nature14956](https://doi.org/10.1038/nature14956)
- 305 Blaauw, M., & Žagar, N. (2018). Multivariate analysis of Kelvin wave seasonal vari-
306 ability in ECMWF L91 analyses. *Atmos. Chem. Phys.*, *18*, 8313-8330. doi: 10
307 [.5194/acp-18-8313-2018](https://doi.org/10.5194/acp-18-8313-2018)
- 308 ESA. (1999). *Atmospheric Dynamics Mission, Reports for Mission Selections*. ESA
309 SP-1233, 4, 155 pp.
- 310 ESA. (2008). *ADM-Aeolus Science Report*. ESA SP-1311, 121 pp.
- 311 Fisher, M., Leutbecher, M., & Kelly, G. (2005). On the equivalence between kalman
312 smoothing and weak-constraint four-dimensional variational data assimilation.
313 *Q. J. R. Meteorol. Soc.*, *131*, 3235-3246.
- 314 Flannaghan, T. J., & Fueglistaler, S. (2012). Tracking Kelvin waves from the equa-
315 torial troposphere into the stratosphere. *J. Geophys. Res.*, *117*. (D21108) doi:
316 [10.1029/2012JD017448](https://doi.org/10.1029/2012JD017448)
- 317 Flannaghan, T. J., & Fueglistaler, S. (2013). The importance of the tropical
318 tropopause layer for equatorial Kelvin wave propagation. *J. Geophys. Res.*,
319 *118*, 5160-5175.
- 320 Fujiwara, M., Suzuki, J., Gettelman, A., Hegglin, M., Akiyoshi, H., & Shibata, K.
321 (2012). Wave activity in the tropical tropopause layer in seven reanalysis
322 and four chemistry climate model data sets. *J. Geophys. Res. - Atmospheres*,
323 *117*(D12). (D12105) doi: [10.1029/2011JD016808](https://doi.org/10.1029/2011JD016808)
- 324 Haiden, T., & Coauthors. (2018). *Evaluation of ECMWF forecasts, including the*
325 *2018 upgrade*. ECMWF Technical memo 831, October 2018. Available from
326 <http://www.ecmwf.int>.
- 327 Kasahara, A. (2020). *3D Normal Mode Functions (NMFs) of a Global Baroclinic*
328 *Atmospheric Model*. Modal View Of Atmospheric Variability: Applications
329 Of Normal-Mode Function Decomposition in Weather and Climate Research.
330 N. Žagar and J. Tribbia, Eds., Springer, Mathematics of Planet Earth Series,
331 Vol.8.
- 332 Kasahara, A., & Puri, K. (1981). Spectral representation of three-dimensional global
333 data by expansion in normal mode functions. *Mon. Wea. Rev.*, *109*, 37-51.
- 334 Kim, H., Caron, J. M., Richter, J. H., & Simpson, I. R. (2020). The Lack of
335 QBO-MJO Connection in CMIP6 Models. *Geophysical Research Letters*,
336 *47*, e2020GL087295. doi: <https://doi.org/10.1029/2020GL087295>
- 337 Kim, J. E., & Alexander, M. J. (2013). Tropical precipitation variability and con-
338 vectively coupled equatorial waves on submonthly time-scales in reanalyses and
339 TRMM. *J. Climate*, *26*, 3013-3030.
- 340 Lean, P., Holm, E. V., Bonavita, M., Bormann, N., McNally, A. P., & Järvinen, H.
341 (2021). Continuous data assimilation for global numerical weather prediction.
342 *Q. J. R. Meteorol. Soc.*, *147*, 273-288.
- 343 Matthews, A., & Madden, R. A. (2000). Observed propagation and structure of the
344 33-h atmospheric Kelvin wave. *J. Atmos. Sci.*, *57*, 3488-3497.

- 345 Park, Y.-Y., Buizza, R., & Leutbecher, M. (2004). TIGGE: preliminary results on
346 comparing and combining ensembles. *Q. J. R. Meteorol. Soc.*, *134*, 2029-2050.
- 347 Podglajen, A., Hertzog, A., Plougonven, R., & Žagar, N. (2014). Assessment of the
348 accuracy of (re)analyses in the equatorial lower stratosphere. *J. Geophys. Res.*,
349 *119*, 11166-11188.
- 350 Reitebuch, O. (2012). *The spaceborne wind lidar mission ADM-Aeolus*. In Atmo-
351 spheric Physics. Schumann U. (Ed.) Research Topics in Aerospace. Springer,
352 Berlin, Heidelberg, pages 815-827. Retrieved from [https://doi.org/10.1007/
353 978-3-642-30183-4_49](https://doi.org/10.1007/978-3-642-30183-4_49)
- 354 Rennie, M., & Isaksen, L. (2020). *The NWP Impact of Aeolus Level-2B Winds at
355 ECMWF*. ECMWF Research Department Technical Memorandum 864. Avail-
356 able from <http://www.ecmwf.int/en/research/publications>. Retrieved from
357 <https://dx.doi.org/10.21957/alift7mhr>
- 358 Rennie, M., & Isaksen, L. (2021). The impact of Aeolus wind retrievals in ECMWF
359 global weather forecasts. *Q. J. R. Meteorol. Soc.*, *147*, submitted.
- 360 Salby, M. L., & Garcia, R. R. (1987). Transient response to localized episodic heat-
361 ing in the tropics. Part I: Excitation and short-time near-field behavior. *J. At-
362 mos. Sci.*, *44*, 458-498.
- 363 Sobel, A., Polvani, N., & Nilsson, J. (2001). The weak temperature gradient approx-
364 imation. *J. Atmos. Sci.*, *58*, 1473-1489.
- 365 Stoffelen, A., Pailleux, J., Källén, E., Vaughan, J. M., Isaksen, L., Flamant, P.,
366 ... Ingmann, P. (2005). The atmospheric dynamic mission for global wind
367 measurements. *Bull. Amer. Meteor. Soc.*, *86*, 73-87.
- 368 Suzuki, J., & Shiotani, M. (2008). Space-time variability of equatorial Kelvin waves
369 and intraseasonal oscillations around the tropical tropopause. *J. Geophys.
370 Res.*, *113*, D16110. doi: 10.1029/2007JD009456
- 371 Suzuki, J., Shiotani, M., & Nishi, N. (2010). Lifetime and longitudinal variability
372 of equatorial Kelvin waves around the tropical tropopause region. *J. Geophys.
373 Res.*, *115*, D03103. doi: 10.1029/2009JD012261
- 374 Tan, D., Andersson, E., De Kloe, J., Marseille, G.-J., Stoffelen, A., Denneulin,
375 P. P. M., ... Nett, H. (2008). The ADM-Aeolus wind retrieval algorithms.
376 *Tellus*, *60 A*, 191-205. doi: 10.1111/j.1600-0870.2007.00285.x
- 377 Tan, D., Andersson, E., Fisher, M., & Isaksen, L. (2007). Observing-system impact
378 assessment using a data assimilation ensemble technique: application to the
379 ADM-Aeolus wind profiling mission. *Q. J. R. Meteorol. Soc.*, *133*, 381-390.
- 380 Tan, D. G. H., & Andersson, E. (2004). *Expected benefit of wind profiles from the
381 ADM-Aeolus in a data assimilation system*. Final report for ESA contract No.
382 15342/01/NL/MM, October 2004.
- 383 Vitart, F., Balsamo, G., Buizza, R., Ferranti, L., Keeley, S., Magnusson, L., ...
384 Weisheimer, A. (2014). *Sub-seasonal predictions*. ECMWF Research De-
385 partment Technical Memorandum n. 734, pp. 47 (available from ECMWF,
386 Shinfield Park, Reading RG2-9AX, UK).
- 387 Šavli, M., Žagar, N., & Anderson, J. (2018). Assimilation of the horizontal line-of-
388 sight winds with a mesoscale EnKF data assimilation system. *Q. J. R. Meteorol.
389 Soc.*, *144*, 2133-2155. doi: 10.1002/qj.3323
- 390 Žagar, N. (2004). Assimilation of equatorial waves by line of sight wind observations.
391 *J. Atmos. Sci.*, *61*, 1877-1893.
- 392 Žagar, N. (2017). A global perspective of the limits of prediction skill of NWP mod-
393 els. *Tellus A*, *69*, 1317573.
- 394 Žagar, N., Andersson, E., Fisher, M., & Untch, A. (2007). Influence of the quasi-
395 biennial oscillation on the ECMWF model short-range forecast errors in the
396 tropical stratosphere. *Q. J. R. Meteorol. Soc.*, *133*, 1843-1853.
- 397 Žagar, N., Blaauw, M., Jesenko, B., & Magnusson, L. (2016). *Diagnosing model
398 performance in the tropics* (Vol. 147). ECMWF Newsletter, available from
399 <http://www.ecmwf.int/publications/newsletters>.

- 400 Žagar, N., Buizza, R., & Tribbia, J. (2015). A three-dimensional multivariate
401 modal analysis of atmospheric predictability with application to the ECMWF
402 ensemble. *J. Atmos. Sci.*, *72*, 4423-4444.
- 403 Žagar, N., Isaksen, L., Tan, D., & Tribbia, J. (2013). Balance properties of the
404 short-range forecast errors in the ECMWF 4D-Var ensemble. *Q. J. R. Meteorol. Soc.*, *139*, 1229-1238.
- 405
406 Žagar, N., Kasahara, A., Terasaki, K., Tribbia, J., & Tanaka, H. (2015). Normal-
407 mode function representation of global 3D datasets: open-access software for
408 the atmospheric research community. *Geosci. Model Dev.*, *8*, 1169-1195.
- 409 Žagar, N., & Szunyogh, I. (2020). Comments on "What Is the Predictability Limit
410 of Midlatitude Weather?". *J. Atmos. Sci.*, *72*(2), 781-785. doi: [https://doi](https://doi.org/10.1175/JAS-D-19-0166.1)
411 [.org/10.1175/JAS-D-19-0166.1](https://doi.org/10.1175/JAS-D-19-0166.1)
- 412 Wallace, J. M., & Gousky, V. E. (1968). Observational evidence of Kelvin waves in
413 the tropical stratosphere. *J. Atmos. Sci.*, *25*, 900-907.
- 414 Wheeler, M., & Kiladis, G. N. (1999). Convectively coupled equatorial waves: analy-
415 sis of clouds and temperature in the wavenumber-frequency domain. *J. Atmos.*
416 *Sci.*, *56*, 374-399.
- 417 Zhang, C. (2005). Madden-Julian oscillation. *Rev. Geophys.*, *43*, 1-36.

Tropical analysis uncertainties and Kelvin waves: what can be learnt from the Aeolus wind profiles?

N. Žagar¹, M. Rennie² and L. Isaksen²

¹Meteorologisches Institut, Universität Hamburg, Germany

²European Centre for Medium Range Weather Forecasts, Reading, UK

An example of the Kelvin wave filtering in the ECMWF model

The Kelvin wave is the slowest eastward-propagating linear wave on the sphere. Its horizontal structure is represented in terms of Hough harmonics whereas the vertical structure is obtained by numerically solving the vertical structure equation for the realistic stability and discretization profiles for the troposphere and stratosphere (Kasahara, 2020; Blaauw & Žagar, 2018; Castanheira & Marques, 2015). Its filtering in operational ECMWF forecasts using the MODES software (Žagar et al., 2015) has been routinely performed since 2014, currently at <https://modes.cen.uni-hamburg.de>. An example of Kelvin wave in the ECMWF model forecasts is shown in Fig. S1 for a single deterministic forecast by the operational system in May 2020 that assimilated Aeolus winds. Forecasts at subsequent days show the vertical KW propagation according to classical linear theory (Andrews et al., 1987). A horizontal line near 33 hPa is added for an easier

visualization of the downward moving wave phase wind over the Indian ocean sector, in evidence of the vertical propagation of energy. The high vertical resolution of the operational ECMWF model resolves an eastward-slanted wave structure in TTL and in the stratosphere. Recent studies of the KW variability using three-dimensional linear theory include Blaauw and Žagar (2018), who described seasonal variability of KWs in TTL in relation to the background winds and stability in ECMWF operational analyses, and Castanheira and Marques (2015), who analyzed KWs coupled to convection.

Other supporting Figures

Tropical zonal winds in the Aeolus and NoAeolus analyses along with their portions associated with the Rossby (or balanced) and non-Rossby (or unbalanced) modes are shown in Figures S2-S4.

References

- Andrews, D. G., Holton, J. R., & Leovy, C. B. (1987). *Middle atmosphere dynamics*. Academic Press, Inc.
- Blaauw, M., & Žagar, N. (2018). Multivariate analysis of Kelvin wave seasonal variability in ECMWF L91 analyses. *Atmos. Chem. Phys.*, *18*, 8313-8330. doi: 10.5194/acp-18-8313-2018
- Castanheira, J., & Marques, C. (2015). Convectively coupled equatorial-wave diagnosis using three-dimensional normal modes. *Quarterly Journal of the Royal Meteorological Society*, *141*(692), 2776–2792. doi: 10.1002/qj.2563
- Kasahara, A. (2020). *3D Normal Mode Functions (NMFs) of a Global Baroclinic Atmo-*

:
spheric Model. Modal View Of Atmospheric Variability: Applications Of Normal-Mode Function Decomposition in Weather and Climate Research. N. Žagar and J. Tribbia, Eds., Springer, Mathematics of Planet Earth Series, Vol.8.

Žagar, N., Kasahara, A., Terasaki, K., Tribbia, J., & Tanaka, H. (2015). Normal-mode function representation of global 3D datasets: open-access software for the atmospheric research community. *Geosci. Model Dev.*, 8, 1169-1195.

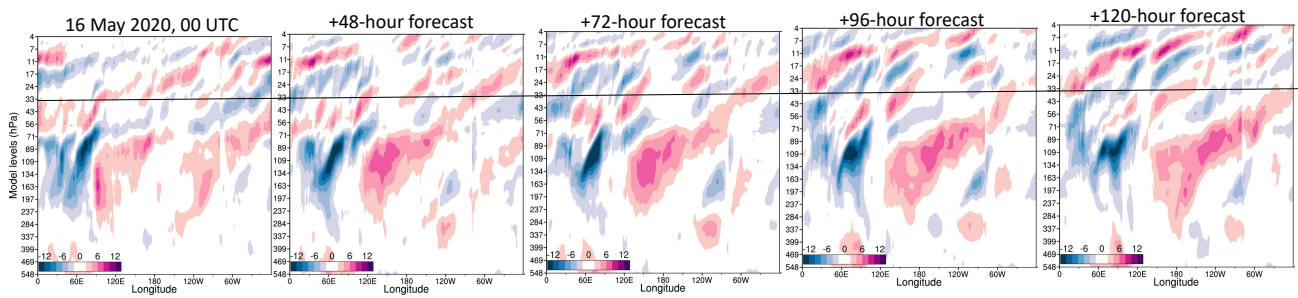


Figure S1. Kelvin wave zonal wind in the operational ECMWF analysis on 16 May 2020, 00 UTC, and in 48-hour, 72-hour, 96-hour and 120-hour forecasts. The zonal wind is averaged over the equatorial belt 15° S – 15° N. Easterlies are in blue and westerlies are in red shades as defined by the colorbar with contouring every 2 m/s. Zero contour is omitted. From <https://modes.cen.uni-hamburg.de>.

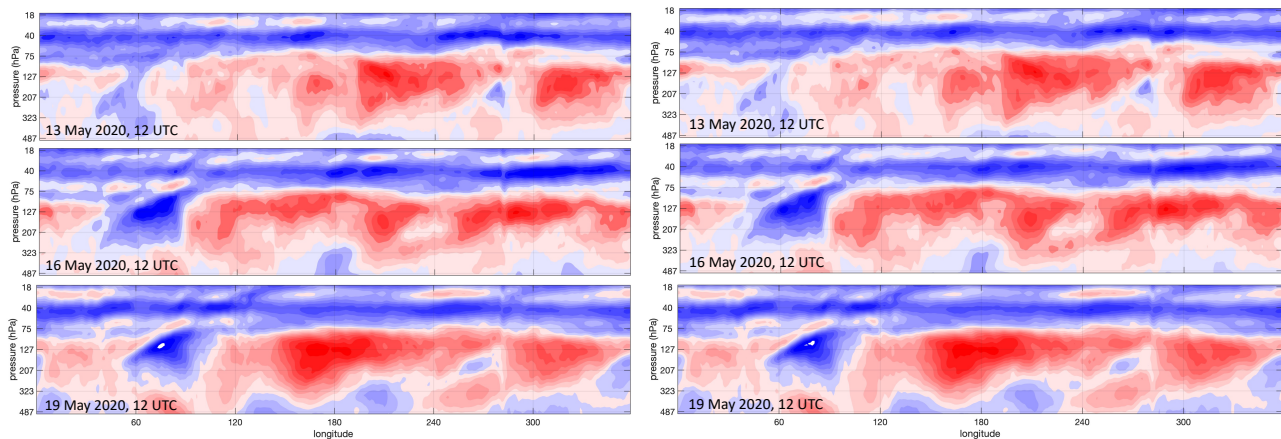


Figure S2. Zonal winds along the equator, averaged over the belt 10° N- 10° S in (left) NoAeolus and (right) Aeolus experiments on 13 May, 16 May and 19 May 2020, 12 UTC. Shading is every 3 m/s, with red shades for westerly winds, and blue shades for easterlies.

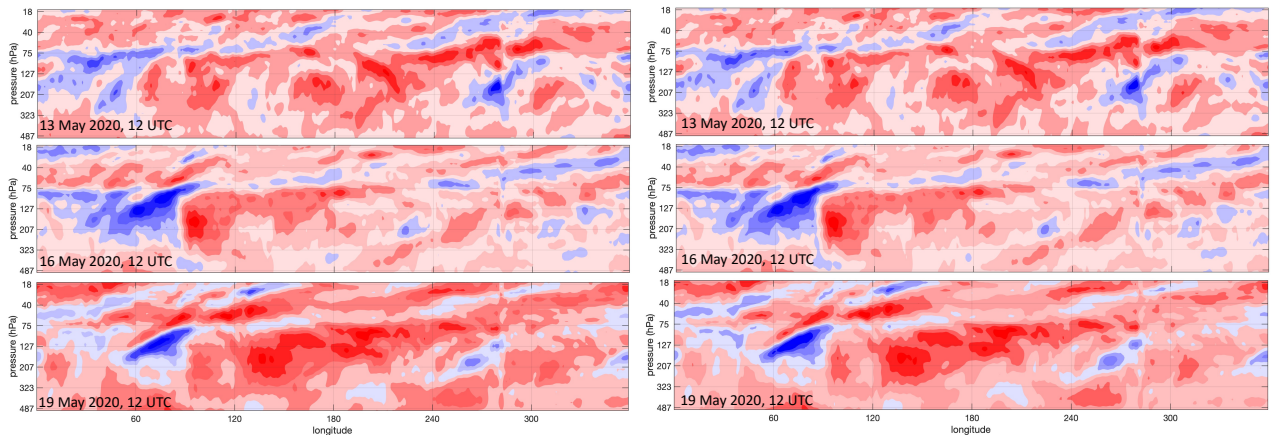


Figure S3. As in Fig. S2 but for the unbalanced (or non-Rossby) zonal winds including the Kelvin and mixed Rossby-gravity zonal winds.

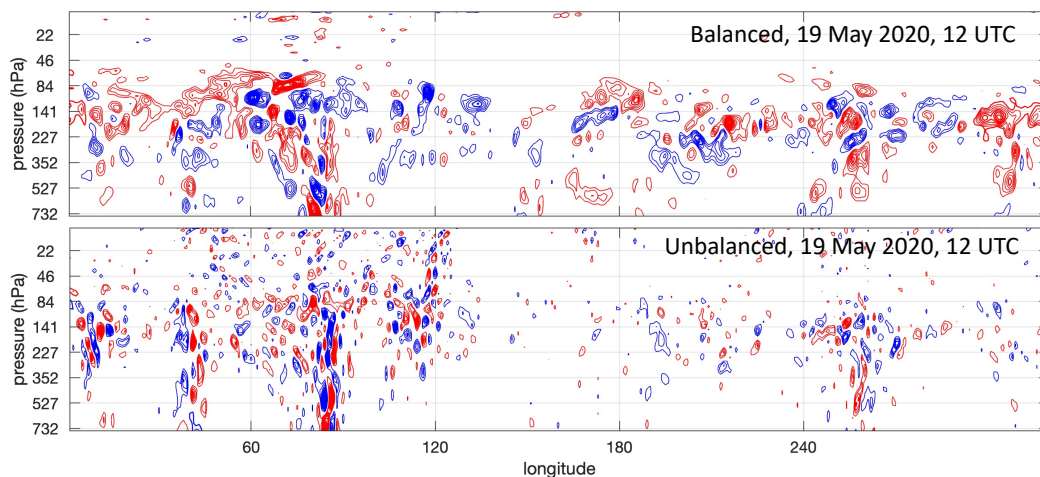


Figure S4. Differences along the equator between the zonal wind in analyses with and without Aeolus winds on 19 May 2020, 12 UTC. Differences are computed separately for balanced (Rossby) and unbalanced (non-Rossby) modes. Contouring is every 0.5 m/s, starting at ± 1 m/s. Red contours for positive, and blue for negative differences.